Inorganic Chemistry

Article

pubs.acs.org/IC

Multimetastability in a Spin-Crossover Compound Leading to Different High-Spin-to-Low-Spin Relaxation Dynamics

Gavin A. Craig,[†] Jose Sánchez Costa,*[,†] Simon J. Teat,[‡] Olivier Roubeau,*[,§] Dmitry S. Yufit,[⊥] Judith. A. K. Howard,[⊥] and Guillem Aromí*[,†]

[†]Departament de Química Inorgànica, Universitat de Barcelona, Diagonal 647, 08028 Barcelona, Spain

[‡]Advanced Light Source, Berkeley Laboratory, 1 Cyclotron Road, Berkeley, California 94720, United States

[§]Instituto de Ciencia de Materiales de Aragón (ICMA), CSIC and Universidad de Zaragoza, Plaza San Francisco s/n, 50009 Zaragoza, Spain

[⊥]Department of Chemistry, Durham University, South Road, Durham DH1 3LE, U.K.

Supporting Information

ABSTRACT: The relaxation kinetics of both the thermally trapped and photoinduced high-spin (HS) states of the spin-crossover compound $[Fe(H_4L)_2](ClO_4)_2{\cdot}H_2O{\cdot}2(CH_3)_2CO$ (**1**) were measured and found to differ significantly. Calorimetry measurements then demonstrated that relaxation of the thermally trapped phase was concurrent with two separate processes, not previously detected as such. Determination of the photogenerated HS structure revealed a new metastable HS state of the system, much closer *structurally* to the low-spin phase than the thermally trapped one. This difference is proposed as the root of the disparate kinetic behavior, which is proposed to require two processes in the case of the structurally more complex thermally trapped state. Therefore, light irradiation is shown as a mechanism to decouple effectively the structural and magnetic phase transitions that occur in **1** during the course of its spin crossover.

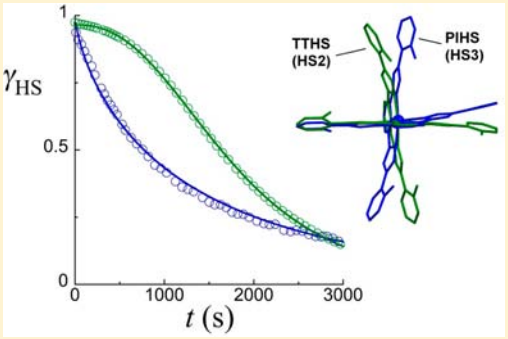

INTRODUCTION

Control of the spin state of Fe^{II} in spin-crossover (SCO) systems constitutes an attractive option for the development of molecule-based switchable devices.[1−4] Such interest stems from the frequent observation of bistability over important temperature intervals of the high-spin (HS; $S = 2$) and low-spin (LS; $S = 0$) magnetic states of this metal ion. Thus, many efforts have focused on enlarging the hysteresis loops and bringing these close to room temperature.[5−9] In this context, another way of exploiting the switching between the two magnetic states of Fe^{II} is trapping a metastable HS state in a controlled manner. A convenient way of achieving this is through the light-induced excited-spin-state trapping (LIESST) effect and its reverse process, triggered through irradiation with light of different energy ranges, typically green and red, respectively.[10,11] Another way to capture a metastable HS state is by rapidly cooling a SCO sample from a temperature where HS is the stable state. The latter process is termed thermally induced excited-spin-state trapping (TIESST).[12] The metastable character of these states leads to their conversion to the LS ground state, following relaxation processes at rates that are strongly influenced by the exact interplay between short- and long-range interactions existing within the crystal lattice of the compound.[11,13,14] An important goal is thus to increase the thermal stability of these HS states. Along these lines, systems that undergo crystallographic phase transitions concomitantly with the thermally induced HS-to-LS transition are particularly interesting. Indeed, because the LIESST effect is essentially a fast electronic transition localized at the active molecules, it is conceivable that in these systems the photoinduced HS (PIHS) state exhibits a crystallographic phase different from that of the high-temperature stable HS state. Indeed, crystallographic symmetry breaking with respect to the high-temperature HS state was detected in the PIHS state of systems that exhibit more than one structural phase transition upon thermal SCO.[15−17] While in these latter cases the LIESST effect caused the tripling of one of the unit cell parameters, more subtle variations of the unit cell parameters and coordination octahedron with respect to the high-temperature HS phase have also been observed after irradiation of a low-temperature LS state.[18,19] In a remarkable crystallographic study, the PIHS state of the compound $[Fe(bapbpy)(NCS)_2]$ [bapbpy = 6,6′-bis(amino-2-pyridyl)-2,2′-bipyridine] was demonstrated to relax through an intermediate metastable phase in an ordered mixed spin state, which coincides with that obtained upon thermally trapping the compound.[20] However, so far, a comparison of the relaxation kinetics from HS to LS of

Received: April 3, 2013
Published: June 4, 2013

   dx.doi.org/10.1021/ic400776x | *Inorg. Chem.* 2013, 52, 7203−7209

crystallographically *different* though magnetically equivalent metastable states is lacking. In a recent paper, the structures and kinetics of relaxation to LS of both the optically induced and thermally trapped metastable HS state of the compound *cis*-[Fe-(picen)$(NCS)_2$] [picen = *N*,*N*′-bis(2-pyridylmethyl)-1,2-ethanediamine] were indeed compared.[21] For this system, the structure of the metastable state is independent of the way in which it was generated and therefore the differences in relaxation kinetics are only subtle. The structural differences between various light-induced and thermally quenched states in the well-known $[Fe(ptz)_6](BF_4)_2$ compound (ptz = 1-propyltetrazole) were recently studied and correlated to the differences in the thermal stability of these states [through their respective critical temperature T(LIESST) and T(TIESST)] but not to any relaxation dynamics.[22] We report here the structure of the PIHS metastable state of the compound $[Fe(H_4L)_2](ClO_4)_2{\cdot}H_2O{\cdot}2(CH_3)_2CO$ {**1**; H_4L = 2,6-bis[5-(2-hydroxyphenyl)pyrazol-3-yl]pyridine},[23,24] which features significant disparities with that of the thermally trapped HS (TTHS) state.[23] This has allowed the observation of differing relaxation kinetics to the LS ground state and a discussion of these differences, for the first time, in light of the different metastable structures.

Compound **1** displays a cooperative spin transition, with an asymmetric hysteresis loop of around 40 K (Figure 1, where χ is the molar paramagnetic susceptibility).[23] A metastable HS state of this compound (HS2) is accessible by thermal trapping and exhibits a high T(TIESST) of 106 K upon warming of the sample at 0.3 K min^{-1} (Figure 1). The structure of HS2 is virtually identical to that of the stable HS state of **1** at 150 and 200 K,[23] once the thermal effects on the structural parameters are considered. The spin transition is concomitant with a disorder−order crystallographic transition of all the acetone molecules and half of the perchlorate anions present in the lattice, as demonstrated by extended single crystal X-ray diffraction studies. The disordered crystallographic phase is maintained upon generation of HS2 by flash cooling, thus, it was considered to be inherent to the HS state independently of the temperature. The present report, revealing the intimate properties of a new metastable state, now photogenerated, demonstrates that this is not the case.

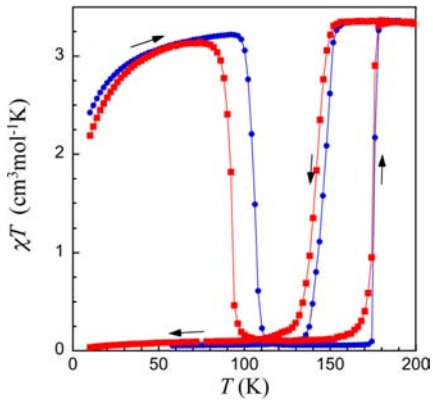

Figure 1. Plots of χT versus T of **1** (χ = molar magnetic susceptibility) after LIESST (red squares) and TIESST (blue dots). The temperature scan rate was ca. 0.3 K min^{-1}.

RESULTS

Photoinduced Metastable HS State of 1 (HS3). A thin sample of **1** was cooled in a SQUID to 10 K at ca. 0.3 K min^{-1}, thereby reaching its LS ground state, and it was then irradiated with light of 500−650 nm, causing full photoexcitation to the metastable HS state (HS3), as shown by the χT versus T curve (Figure 1). The sample was protected with grease, which makes the excitation less efficient but prevents crystallite orientation effects observed on a similar free sample (Figure S1 in the Supporting Information, SI). On the other hand, when a thicker sample of **1** was used, the excitation was much less efficient (Figure S1 in the SI). Once irradiation was stopped, the temperature was raised at 0.3 K min^{-1} (Figure 1), causing an increase of χT from 2.18 cm^3 K mol^{-1} at 10 K to 3.1 cm^3 K mol^{-1} at 70 K, as expected for a full HS iron(II) complex under zero field splitting.[25] Above ca. 75 K, the sample enters the thermally activated regime of relaxation to the LS state. The value of T(LIESST) is 92 K (Figure S2 in the SI), thus more than 10 K lower in temperature than T(TIESST),[10] the thermally activated relaxation temperature of the HS2 state. Upon continued heating, the static LS-to-HS thermal SCO was induced almost exactly as previously observed when the sample in the LS ground state was heated. Attempts to induce the reverse-LIESST phenomenon[26,27] were made by irradiating the sample of **1** with various ranges of red light (see Figure S3 in the SI), with no appreciable response. A possible explanation for this is[11,28] (i) the process is highly inefficient because of low quantum yield, competition with LIESST, and/or absorption effects or (ii) the ^5E state reached by irradiation lies below the ^3T state, preventing intersystem crossing and instead facilitating relaxation back to the metastable $^5T_2$ state HS3.

The kinetics of relaxation of the PIHS metastable state of **1** (HS3) were then investigated through magnetic measurements on a thin sample. Figure 2 shows the isothermal time evolution of the fraction of the HS3 state of **1**, as fully generated by irradiation of the LS ground state at 10 K and then rapidly brought to various temperatures below T(LIESST). These plots approximate to first-order exponential kinetics, although the lowest-temperature data suggest the presence of a short induction time or slower initial step to relaxation. These *quasi*-first-order relaxation dynamics are in contrast with the anticipated sigmoidal behavior typical of cooperative systems.[28−31] While the experimental data are not well reproduced by a single-exponential law (Figure S4 in the SI), the use of a stretched exponential function does allow one to reach a good agreement (Figure 2), indicating that the deviations from single exponentials likely originate from a distribution of relaxation rates. Such an effect is, in fact, often observed in SCO systems and may result from inhomogeneities either intrinsic to the material and related to distortions,[32] disorder, or defects[33−35] or due to gradients created during broad-band irradiation.[11] The stretched exponential is indeed widely used to fit relaxation processes in disordered systems,[36] although it does not model the origin of inhomogeneities. The characteristic times τ derived from the stretched-exponential fits used here turned out to be very similar to those obtained by taking the time when $\gamma_{HS} = 1/e$ (γ_{HS} is the fraction of molecules in the HS state), i.e., assuming a pure single-exponential decay. This strongly indicates that relaxation kinetics of the PIHS of **1** follow a simple exponential behavior but are significantly affected by inhomogeneities. The resulting k_{HL} versus $1/T$ plot ($k_{HL} = 1/\tau$ is the HS-to-LS relaxation rate; Figure S5 in the SI)

dx.doi.org/10.1021/ic400776x | *Inorg. Chem.* 2013, 52, 7203−7209

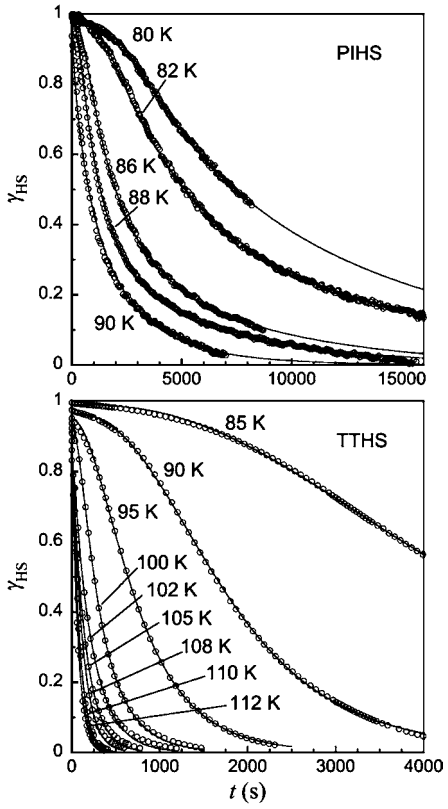

Figure 2. HS-to-LS relaxation kinetics of **1** at various temperatures, after LIESST (PIHS, top) and thermal trapping (TTHS, bottom). Full lines are the best fits to a stretched exponential (top) or eqs 1 and 2 (bottom).

provides an estimated mean activation energy of E_a = 1069 cm^{-1} and an associated frequency factor of A_{HL} = 2.04 × 10^4 s^{-1}.

Relaxation of the Thermally Trapped Metastable HS State of 1 (HS2). The relaxation dynamics of the TTHS state of **1** (HS2) were also studied by the same method. Thus, the metastable HS2 state was first generated by flash cooling the sample to 10 K, which leads to a fully magnetically trapped system (Figure 1).[23] Then, the isothermal relaxation was followed for temperatures in the 85−112 K range (Figure 2, bottom). Quite remarkably, the process of relaxation of HS2 was found to differ significantly from that of HS3 in that the curves deviate now markedly from a simple exponential behavior, especially at the lowest temperatures, approaching now a sigmoidal shape. Thus, the relaxation isotherms of the TTHS state exhibit a very apparent initial period of induction before initiating an accelerated decay. Interestingly, however, the higher-temperature curves are reproduced with a simple exponential function, and the characteristic times and constant rates of relaxation obtained by taking the τ values as the time where γ_{HS} = 1/e are very similar to those found for the relaxation of HS3. Indeed, for HS2, values of E_a = 1129 cm^{-1} and A_{HL} = 3.58 × 10^4 s^{-1} were extracted (Figure S6 in the SI).

The isothermal HS2-to-LS state transition process was also followed by single-crystal X-ray diffraction. For this, it was particularly useful to examine the isothermal evolution of the cell parameters, especially those that experience the largest changes upon SCO, which in this case is α (for HS to LS, $\Delta\alpha$ = +2.06°).[23] Crystallographic analysis of the relaxation of the TTHS state is consistent with the observations made from magnetic measurements and confirms the coupling of the spin and crystallographic phase transitions.

In particular, a delay in the cell parameter evolution toward the LS phase is evident in the lower-temperature set of data (93 K), matching the evolution of γ_{HS} (Figure 3), which is not

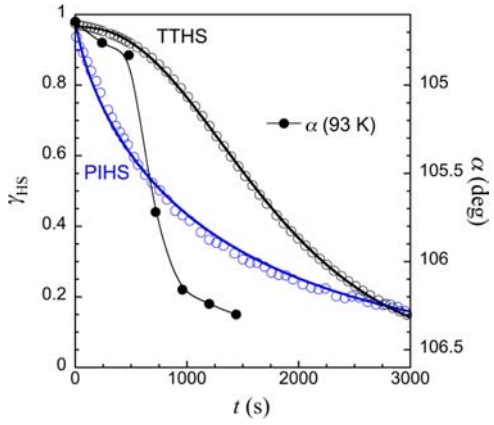

Figure 3. Relaxation kinetics of the PIHS and TTHS at 90 K, emphasizing their differing shape. The evolution of the α angle of the TTHS cell at 93 K is also shown, evidencing an initial delay in the cell evolution toward that of the LS. Note that the α-axis limits coincide with the values for the full HS and LS ground states.

detectable at higher temperatures (102 K; Figure S7 in the SI). This delay in the relaxation of HS2, not observed for HS3, suggests the occurrence of an additional process of rearrangement in the former during its transit to the LS state. To unveil the possible presence of two separate processes in the relaxation from the TTHS state, not detected in the χT versus T curve (Figure 1), we have used differential scanning calorimetry (DSC). Thus, crystals of **1** in a DSC aluminum pan were flash-cooled by immersion in liquid N_2, and the pan was rapidly transferred to the DSC sample space ready at 93 K. The subsequent heat flow measured upon warming at 10 K min^{-1} clearly exhibits two separate exothermic humps at ca. 119 and 126 K, respectively, which are not detected if the same measurement is performed on a nonquenched sample (i.e., after cooling the sample at a much slower rate; Figure 4). The total

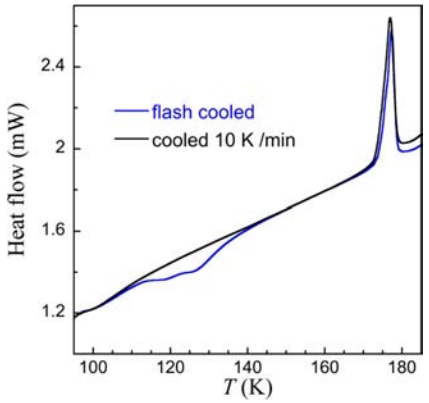

Figure 4. DSC traces warming at 10 K min^{-1} after flash cooling to 77 K and after cooling to 93 at 10 K min^{-1}. Note the two separate anomalies at ca. 119 and 126 K that are present only after flash cooling, as well as the similarity in the peak associated with the thermal LS-to-HS SCO of **1** at around 178 K.

dx.doi.org/10.1021/ic400776x | Inorg. Chem. 2013, 52, 7203−7209

enthalpy, ca. 3.1 kJ mol^{-1}, is similar to that associated with the thermal HS-to-LS transition,[23] and the anomalies are thus due to the thermal relaxation of the metastable state HS2 to the LS ground state.[37] Bearing in mind the disorder present in the HS2 lattice, the two involved processes evidenced by the DSC data may then be reasonably posited as first a structural transition from the disordered HS2 state to an intermediate HS2′ state, perhaps ordered, followed by the HS-to-LS transformation. This assumption does not warrant the use of a self-accelerated relaxation model, typically used in cooperative SCO systems because here the initial step seems to be a structural transformation to an intermediate HS state. In support of this hypothesis, the relaxation curves of the TTHS (HS2) state were very satisfactorily reproduced (full lines in Figure 2, bottom) by the phenomenological model in eqs 1 and 2

$$k_{app}(t, T) = k_{HL}(T)\{1 - \exp[-k'(T)\,t]\} \quad (1)$$

$$\gamma_{HS}(t, T) = \gamma_{HS}(t = 0, T)\exp[-k_{app}(T, T)\,t] \quad (2)$$

where $k'(T)$ describes the rate of the initial structural transformation and $k_{HL}(T)$ is the relaxation constant of a hypothetical intermediate HS2′ state. Remarkably, the derived k_{HL} values are in perfect agreement with those found for HS3. Both sets of parameters correspond to exponential decays that merge into a common Arrhenius law with E_a = 978 cm^{-1} and $A_{HL} = 4.24 \times 10^3$ s^{-1} (Figure 5). The apparent relaxation rate k_{app} of the TTHS system strongly departs from this law for temperatures at which the initial structural transformation is slow and thus dominant.

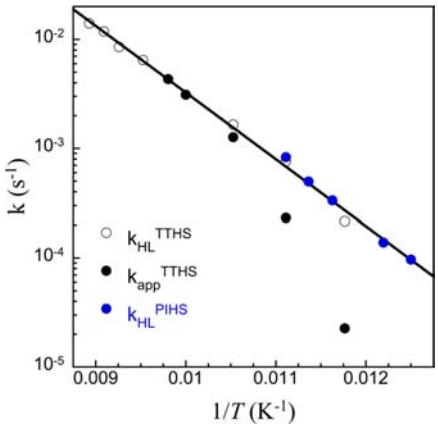

Figure 5. Semilogarithmic plot of the relaxation constants k derived from the relaxation kinetics versus $1/T$. The full line is a fit of k_{HL}, from both the PIHS and TTHS states, to a common Arrhenius law. k_{app} values are for t = 1000 s; the departure from the Arrhenius law is even more pronounced for shorter times.

Crystallographic Comparison of the Metastable States. In order to investigate the possible structural origin of these marked differences in relaxation dynamics, access to crystallographic information on the HS3 state was of vital importance. The PIHS of **1** (HS3) was generated at 30 K by irradiation of a single crystal for 60 min with laser light of 532 nm. Subsequently, the molecular structure at this temperature was determined by single-crystal X-ray diffraction. This experiment showed that the HS3 state remains in the triclinic space group $P\bar{1}$ as in all of the previously obtained structures of **1** (HS and LS ground states as well as HS2).[23]

Table 1. Crystallographic Details of the Metastable HS Phases of Compound 1 (HS2 and HS3) and Its HS and LS Ground States

	HS3 (PIHS)	HS2 (TTHS)	LS	HS
T/K	30(2)	100(2)	100(2)	200(2)
cryst syst		triclinic		
space group		$P\bar{1}$		
a/Å	12.262(5)	12.247(2)	12.326(3)	12.310(3)
b/Å	13.385(5)	13.385(3)	13.513(3)	13.442(3)
c/Å	17.217(5)	17.355(4)	17.269(4)	17.399(4)
α/deg	104.127(5)	104.60(3)	106.63(3)	104.57(3)
β/deg	98.450(5)	99.12(3)	98.50(3)	99.29(3)
γ/deg	106.134(5)	105.47(3)	106.36(13)	105.44(3)
V/Å^3	2561.5(16)	2574.4(12)	2560.5(13)	2604.1(13)
av. Fe−N/Å	2.169	2.162	1.966	2.167
octahedral volume/Å^3	12.508	12.419	9.741	12.484
Σ/deg	147.90	144.26	100.52	145.85
Φ/deg	176.40	177.05	178.53	177.01
θ/deg	73.99	74.66	77.17	74.94
Θ/deg	471.89	464.04	311.17	469.18
Ac1 disorder	1:0	0.3:0.7	1:0	0.3:0.7
Ac2 disorder (C3S:C3SA)	0.67:0.33	0.4:0.6	1:0	0.4:0.6
ClO_4^- disorder (O9:O9A)	1:0	0.8:0.2	1:0	0.8:0.2

Table 1 summarizes the relevant crystallographic parameters of the HS and LS ground-state structures, together with those for HS2 and HS3 (see also Tables S1 and S2 in the SI). The asymmetric unit contains one $[Fe(H_4L)_2]^{2+}$ cation, two ClO_4^- anions, two molecules of acetone, and one molecule of water (Figure 6 shows only the cation). The H_4L ligands use their

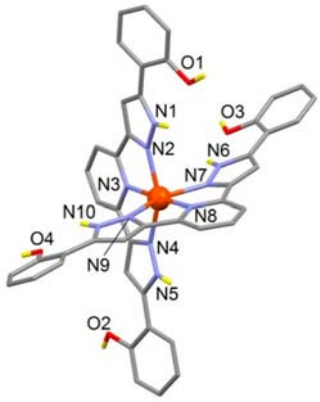

Figure 6. Representation of the $[Fe(H_4L)_2]^{2+}$ cation present in **1**. Only the hydrogen atoms on heteroatoms are shown.

three nitrogen-donor atoms to bind the Fe^{II} center in a meridional fashion and impart a distorted octahedral coordination environment, with an average Fe−N distance (2.169 Å) that confirms the HS character of this phase. The cations are disposed in sheets cemented by a network of $\pi\cdots\pi$ and C−H$\cdots\pi$ interactions involving the H_4L moieties (Figure S8 and Table S1 in the SI), known as the "terpy embrace",[38−40] as seen for the other phases of complex **1**[23] and its close derivatives.[41] These sheets are stacked by means of hydrogen bonds involving the OH and NH moieties from the complexes, via the perchlorate ions, together with additional $\pi\cdots\pi$ contacts

dx.doi.org/10.1021/ic400776x | Inorg. Chem. 2013, 52, 7203−7209

(Figures S9 and S10 and Tables S2 and S3 in the SI), also seen previously.[23] A detailed comparison of this structure with these already available reveals important differences. The most remarkable relates to the crystallographic disorder (Figure 7, bottom); the structure of HS3 exhibits almost no disorder, with only the methyl group of one acetone molecule distributed over two positions in the 0.33:0.67 ratio. By contrast, all of the previously obtained structures of **1** *in the HS state* (i.e., the stable HS states at 150 and 200 K and HS2) feature both acetone molecules disordered over two sites, in 0.4:0.6 and 0.3:0.7 ratios, respectively, and one disordered perchlorate anion, with an occupancy ratio of 0.8:0.2.[23] It must be recalled, however, that in the structures of the LS ground state of **1**, all of the species are *fully ordered*, at both 100 and 150 K. Therefore, from this point of view, the PIHS state HS3 is crystallographically much closer to the LS ground state than is the thermally trapped state HS2. In addition to this, a comparison of the cell parameters of both metastable states shows that the unit cell of the PIHS closely resembles that of the LS ground state, considering the effect of thermal contraction (Table 1). In focusing on the structure of the $[Fe(H_4L)_2]^{2+}$ cation, it is observed that both structures exhibit noticeable differences in the conformation of the H_4L ligands, especially at their wings, where interaction with acetone and the perchlorate species occurs. This has little impact on the local parameters around the Fe^{II} center (Table 1). Thus, the parameters θ and Φ,[42] which measure distortion of the shape of the cation in HS3, are slightly further away from the ideal values of 90° and 180°, respectively, than those in HS2. This small increased distortion is also seen in the parameters Σ and Θ,[43−45] which reflects the extent of deviation of the cis N−Fe−N angles from 90° and the extent of the twist away from octahedral symmetry, respectively.

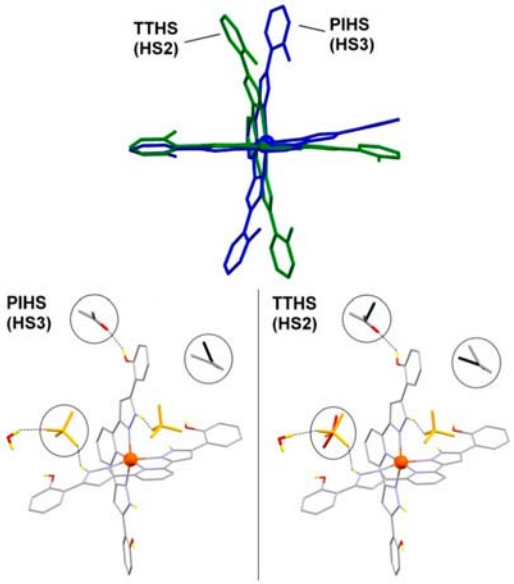

Figure 7. (top) Superposition of the $[Fe(H_4L)_2]^{2+}$ cations of the PIHS (blue) and TTHS (green) metastable states of **1**. (bottom) Representation of the asymmetric unit of both metastable states of **1**, emphasizing the difference in ordering of two molecules of acetone and one perchlorate anion (circled). Color code: C, gray (or black); O, red (or orange); Cl (from ClO_4^-), orange; N, purple; H, yellow; Fe, dark-orange balls. Only hydrogen atoms on heteroatoms are shown. Intermolecular hydrogen bonds are marked as dashed lines.

DISCUSSION

The above analysis reveals that the crystallographic differences between the two available metastable phases of **1**, HS2 and HS3, can explain their differing dynamics of relaxation to the LS ground state. Specifically, the fact that HS3 exhibits almost no crystallographic disorder and a unit cell similar to that of the LS state implies that a relevant part of the crystallographic phase transition coupled with the SCO does not need to take place here for relaxation to the LS state. On the contrary, the metastable state HS2 presents all of the disorder inherent to the stable HS state of **1** and more removed unit cell parameters with respect to the LS state; thus, the crystallographic transition consisting of ordering of all of the species, necessary to reach the LS, has to occur in its entirety, which explains to a large extent the induction time observed in the relaxation dynamics of this state. It is very likely that during the process of relaxation from HS2 to LS, the system passes through a more ordered transient crystallographic phase very close to HS3 (denoted as a hypothetical HS2′ state; see above). This additional crystallographic transition, suggested by the calorimetric data, could be the reason that T(LIESST) is 10 K lower than T(TIESST). On the other hand, the fact that the molecular geometry of HS3 is slightly more removed from that of the final LS ground state than HS2 (longer Fe−N distances and a more distorted coordination polyhedron) signifies that the former electronic state is less stable. This leads to a larger zero-point-energy difference,[29,30] $\Delta H^\circ_{HL} = H^\circ_{HS} - H^\circ_{LS}$, for the PIHS metastable state than for the TTHS. However, once the exponential regime has been reached, relaxation occurs at the same speed for both metastable states; therefore, at that stage, both systems must have evolved to render their ΔH°_{HL} values very similar.

CONCLUSION

In light of the data presented here, compound **1** is a clear example of a system in which the LIESST effect induces fast changes affecting primarily the local molecular environment of the spin-active species while affecting little other crystallographic changes seen to accompany the thermal SCO process. This signifies that using light allows the almost complete decoupling of the crystallographic phase transition from the magnetic phase transition, which could not be differentiated in previous investigations on the transition properties of this compound. This is demonstrated for the first time by the differences in the relaxation dynamics between HS2 and HS3, in light of the respective structures of these metastable states, compared with the structures of the ground state in the HS as well as LS.

EXPERIMENTAL SECTION

Synthesis. The ligand 2,6-bis[5-(2-hydroxyphenyl)pyrazol-3-yl]-pyridine (H_4L) was synthesized as previously described by our group.[24] Complex **1** was synthesized as recently published.[23]

SQUID Magnetometry. Experiments were performed using either a Quantum Design MPMS-5S or MPMS-XL SQUID magnetometers and the Quantum Design fiber-optic setup (FOSH), all through the Servicio General de Apoyo a la Investigación−SAI, Universidad de Zaragoza. The applied field was 1 T throughout the whole study. The light source was a xenon lamp equipped with sets of short- and long-pass filters. Either large and thick orange block crystals or a thin layer of a slightly pressed polycrystalline orange sample was used for the irradiation studies. In the former case, called the thick sample, the crystals were taken out of their mother liquor, put in the FOSH holder with some solution, and allowed to fall to the bottom part of the holder. The small amount of solvent was then removed by absorbing it

dx.doi.org/10.1021/ic400776x | Inorg. Chem. 2013, 52, 7203−7209

with a small piece of absorbing paper. The mass was ca. 1.72 mg. For the latter case, called the thin sample, two sets of measurements were performed with respectively ca. 0.30 mg of the polycrystalline orange sample and ca. 0.40 mg covered with a little Paratone N grease to prevent orientation effects. Extended relaxation studies were made on the former because of the comparatively longer excitation times required in the latter. Data have been corrected for the signal of the empty FOSH, measured prior to these measurements in the same applied field, and for diamagnetism of the sample (7×10^{-4} cm^3 mol^{-1}).

DSC. DSC experiments were performed with a differential scanning calorimeter Q1000 with the LNCS accessory from TA Instruments. The temperature and enthalpy scales were calibrated with a standard sample of indium, using its melting transition (156.6 °C, 3296 J mol^{-1}). Measurements were carried out using aluminum pans. A few crystals of **1** (ca. 0.5 mg) were covered with a little Paratone N grease within the aluminum pan, which was simply covered and not crimped. An empty pan in the same uncrimped geometry was used as the reference.

X-ray Crystallography. Single-crystal X-ray diffraction data were collected on a Bruker SMART-CCD 1K diffractometer (ω scan, 0.3°/frame) equipped with a Helix (Oxford Cryosystems) open-flow helium cryostat using graphite-monochromated Mo Kα radiation (λ = 0.71073 Å). A green laser (λ = 532 nm) mounted on a special attachment[46] was used for in situ irradiation (1 h) of the crystal without changing the temperature. The structure was solved by direct methods and refined by full-matrix least squares on F^2 for all data using *SHELXTL*[47] and *OLEX2*[48] software. All non-hydrogen atoms were refined with anisotropic displacement parameters. Hydrogen atoms were placed in calculated positions and refined in the riding mode. The CIF file has also been deposited with the Cambridge Crystallographic Data Centre as supplementary publication CCDC 921488.

■ ASSOCIATED CONTENT

Supporting Information

X-ray crystallographic data in CIF format, complementary photomagnetic SQUID measurements, larger versions of the constituent figures shown in Figure 2, and additional crystal packing diagrams. This material is available free of charge via the Internet at http://pubs.acs.org.

■ AUTHOR INFORMATION

Corresponding Author

*E-mail: guillem.aromi@qi.ub.es (G.A.), josesanchezcosta@gmail.com (J.S.C.), roubeau@unizar.es (O.R.).

Notes

The authors declare no competing financial interest.

■ ACKNOWLEDGMENTS

G.A. thanks the Generalitat de Catalunya for the prize ICREA Academia 2008 and the ERC for a Starting Grant (258060 FuncMolQIP). The authors thank the Spanish MCI for Grants CTQ2009-06959 (to J.S.C., G.A.C., and G.A.) and MAT2011-24284 (to O.R.). The Advanced Light Source is supported by the Director, Office of Science, Office of Basic Energy Sciences, of the U.S. Department of Energy under Contract DE-AC02-05CH11231. The RSC is thanked for a Journals Grant to International Authors (J.S.C., D.S.Y., J.A.K.H.).

■ REFERENCES

(1) Bousseksou, A.; Molnár, G.; Salmon, L.; Nicolazzi, W. *Chem. Soc. Rev.* **2011**, *40*, 3313−3335.
(2) Gamez, P.; Costa, J. S.; Quesada, M.; Aromí, G. *Dalton Trans.* **2009**, 7845−7853.
(3) Gütlich, P.; Garcia, Y.; Goodwin, H. A. *Chem. Soc. Rev.* **2000**, *29*, 419−427.
(4) Gütlich, P.; Hauser, A.; Spiering, H. *Angew. Chem., Int. Ed.* **1994**, *33*, 2024−2054.
(5) Bartual-Murgui, C.; Ortega-Villar, N. A.; Shepherd, H. J.; Muñoz, M. C.; Salmon, L.; Molnár, G.; Bousseksou, A.; Real, J. A. *J. Mater. Chem.* **2011**, *21*, 7217−7222.
(6) Létard, J.-F.; Guionneau, P.; Codjovi, E.; Lavastre, O.; Bravic, G.; Chasseau, D.; Kahn, O. *J. Am. Chem. Soc.* **1997**, *119*, 10861−10862.
(7) Niel, V.; Martinez-Agudo, J. M.; Muñoz, M. C.; Gaspar, A. B.; Real, J. A. *Inorg. Chem.* **2001**, *40*, 3838−3839.
(8) Roubeau, O. *Chem.—Eur. J.* **2012**, *18*, 15230−15244.
(9) Weber, B.; Bauer, W.; Obel, J. *Angew. Chem., Int. Ed.* **2008**, *47*, 10098−10101.
(10) Létard, J. F. *J. Mater. Chem.* **2006**, *16*, 2550−2559.
(11) Hauser, A. *Top. Curr. Chem.* **2004**, *234*, 155−198.
(12) Marchivie, M.; Guionneau, P.; Létard, J. F.; Chasseau, D.; Howard, J. A. K. *J. Phys. Chem. Solids* **2004**, *65*, 17−23.
(13) Money, V. A.; Carbonera, C.; Elhaik, J.; Halcrow, M. A.; Howard, J. A. K.; Létard, J. F. *Chem.—Eur. J.* **2007**, *13*, 5503−5514.
(14) Hauser, A.; Vef, A.; Adler, P. *J. Chem. Phys.* **1991**, *95*, 8710−8717.
(15) Bréfuel, N.; Collet, E.; Watanabe, H.; Kojima, M.; Matsumoto, N.; Toupet, L.; Tanaka, K.; Tuchagues, J. P. *Chem.—Eur. J.* **2010**, *16*, 14060−14068.
(16) Bréfuel, N.; Watanabe, H.; Toupet, L.; Come, J.; Matsumoto, N.; Collet, E.; Tanaka, K.; Tuchagues, J. P. *Angew. Chem., Int. Ed.* **2009**, *48*, 9304−9307.
(17) Shih, C. H.; Sheu, C. F.; Kato, K.; Sugimoto, K.; Kim, J.; Wang, Y.; Takata, M. *Dalton Trans.* **2010**, *39*, 9794−9800.
(18) MacLean, E. J.; McGrath, C. M.; O'Connor, C. J.; Sangregorio, C.; Seddon, J. M. W.; Sinn, E.; Sowrey, F. E.; Teat, S. L.; Terry, A. E.; Vaughan, G. B. M.; Young, N. A. *Chem.—Eur. J.* **2003**, *9*, 5314−5322.
(19) Money, V. A.; Evans, I. R.; Halcrow, M. A.; Goeta, A. E.; Howard, J. A. K. *Chem. Commun.* **2003**, 158−159.
(20) Pillet, S.; Bendeif, E.; Bonnet, S.; Shepherd, H. J.; Guionneau, P. *Phys. Rev. B* **2012**, *86*, 064106.
(21) Létard, J. F.; Asthana, S.; Shepherd, H. J.; Guionneau, P.; Goeta, A. E.; Suemura, N.; Ishikawa, R.; Kaizaki, S. *Chem.—Eur. J.* **2012**, *18*, 5924−5934.
(22) Kusz, J.; Zubko, M.; Neder, R. B.; Gutlich, P. *Acta Crystallogr.* **2012**, *B68*, 40−56.
(23) Craig, G. A.; Costa, J. S.; Roubeau, O.; Teat, S. J.; Aromí, G. *Chem.—Eur. J.* **2011**, *17*, 3120−3127.
(24) Craig, G. A.; Barrios, L. A.; Costa, J. S.; Roubeau, O.; Ruiz, E.; Teat, S. J.; Wilson, C. C.; Thomas, L.; Aromí, G. *Dalton Trans.* **2010**, *39*, 4874−4881.
(25) Halcrow, M. A. *Chem. Soc. Rev.* **2008**, *37*, 278−289.
(26) Hauser, A. *J. Chem. Phys.* **1991**, *94*, 2741−2748.
(27) Hauser, A. *Chem. Phys. Lett.* **1986**, *124*, 543−548.
(28) Hauser, A. *Coord. Chem. Rev.* **1991**, *111*, 275−290.
(29) Hauser, A.; Enachescu, C.; Daku, M. L.; Vargas, A.; Amstutz, N. *Coord. Chem. Rev.* **2006**, *250*, 1642−1652.
(30) Hauser, A. *Chem. Phys. Lett.* **1992**, *192*, 65−70.
(31) Hauser, A. *Comments. Inorg. Chem.* **1995**, *17*, 17−40.
(32) Bonhommeau, S.; Bréfuel, N.; Pálfi, V. K.; Molnár, G.; Zwick, A.; Salmon, L.; Tuchagues, J.-P.; Sánchez Costa, J.; Létard, J.-F.; Paulsen, H.; Bousseksou, A. *Phys. Chem. Chem. Phys.* **2005**, *7*, 2909−2914.
(33) Roubeau, O.; deVos, M.; Stassen, A. F.; Burriel, R.; Haasnoot, J. G.; Reedijk, J. *J. Phys. Chem. Solids* **2003**, *64*, 1003−1013.
(34) Spiering, H.; Kohlhaas, T.; Romstedt, N.; Hauser, A.; Bruns-Yilmaz, C.; Kusz, J.; Gutlich, P. *Coord. Chem. Rev.* **1999**, *192*, 629−647.
(35) Spiering, H.; Willenbacher, N. *J. Phys.: Condens. Matter* **1989**, *1*, 10089−10105.
(36) Phillips, J. C. *Rep. Prog. Phys.* **1996**, *59*, 1133.
(37) The temperatures of these anomalies (119 and 126 K) are slightly higher with respect to T(TIESST), which is due to the faster rate used. A slower rate indeed shifts the heat flow anomaly to lower temperatures. However, it also results in the merging of both anomalies.

(38) Scudder, M. L.; Craig, D. C.; Goodwin, H. A. *CrystEngComm* **2005**, *7*, 642−649.
(39) McMurtrie, J.; Dance, I. *CrystEngComm* **2005**, *7*, 216−229.
(40) Scudder, M. L.; Goodwin, H. A.; Dance, I. G. *New J. Chem.* **1999**, *23*, 695−705.
(41) Craig, G. A.; Costa, J. S.; Roubeau, O.; Teat, S. J.; Aromí, G. *Chem.—Eur. J.* **2012**, *18*, 11703−11715.
(42) Holland, J. M.; McAllister, J. A.; Kilner, C. A.; Thornton-Pett, M.; Bridgeman, A. J.; Halcrow, M. A. *J. Chem. Soc., Dalton Trans.* **2002**, 548−554.
(43) Marchivie, M.; Guionneau, P.; Létard, J.-F.; Chasseau, D. *Acta Crystallogr.* **2005**, *B61*, 25−28.
(44) Guionneau, P.; Marchivie, M.; Bravic, G.; Létard, J.-F.; Chasseau, D. *Top. Curr. Chem.* **2004**, *234*, 97−128.
(45) McCusker, J. K.; Rheingold, A. L.; Hendrickson, D. N. *Inorg. Chem.* **1996**, *35*, 2100−2112.
(46) Goeta, A. E.; Thompson, A. L.; Beeby, A. *J. Appl. Crystallogr.* **2004**, *37*, 652−653.
(47) Sheldrick, G. M. *Acta Crystallogr.* **2008**, *A64*, 112−122.
(48) Dolomanov, O. V.; Bourhis, L. J.; Gildea, R. J.; Howard, J. A. K.; Puschmann, H. *J. Appl. Crystallogr.* **2009**, *42*, 339−341.

dx.doi.org/10.1021/ic400776x | *Inorg. Chem.* 2013, 52, 7203−7209